

1 Wall loss of semi-volatile organic compounds in a Teflon bag chamber 2 for the temperature range of 262-298 K: mechanistic insight on 3 temperature dependence

4 Longkun He¹, Wenli Liu², Yatai Li^{1,3}, Jixuan Wang¹, Mikinori Kuwata², Yingjun Liu¹

5 ¹State Key Joint Laboratory of Environmental Simulation and Pollution Control, College of Environmental Sciences and
6 Engineering, Peking University, Beijing, 100871, China

7 ²Department of Atmospheric and Oceanic Sciences and Laboratory for Climate and Ocean-Atmosphere Studies, School of
8 Physics, Peking University, Beijing 100871, China

9 ³Now at College of Public Health, Zhengzhou University, Zhengzhou, 450001, China

10 *Correspondence to:* Mikinori Kuwata (kuwata@pku.edu.cn), Yingjun Liu (yingjun.liu@pku.edu.cn)

11
12 **Abstract.** Teflon bag chambers have long been used for investigating atmospheric chemical processes, including secondary
13 organic aerosol formation. The wall-loss process of gas-phase species in Teflon bag chambers has typically been investigated
14 at around room temperature. Recent laboratory studies started employing Teflon bag chambers at sub-273 K conditions for
15 simulating wintertime and upper tropospheric environments. However, temperature dependence in vapor wall-loss processes
16 of semi-volatile organic compounds (SVOCs) in a Teflon bag chamber has not well been investigated. In this study, we
17 experimentally investigated wall-loss process of C₁₄-C₁₉ *n*-alkanes in a 1 m³ Teflon bag for the temperature range of 262 to
18 298 K. Enhanced wall losses of the tested *n*-alkanes were observed following the decrease in temperature. For instance, 65%
19 of C₁₄ *n*-alkane was lost to the wall 15 hours after injection at room temperature, while the corresponding value was 95% at
20 262 K. The experimental data were analyzed using the two-layer kinetic model, which considers both absorption of gas phase
21 species to the surface layer of Teflon wall and diffusion to the inner layer. The experimental data demonstrated that absorption
22 of gas phase species by the surface layer enhanced at lower temperature. The temperature dependence in absorption was well
23 accounted using the equilibrium dissolution model of organic compounds to the Teflon surface by considering reduced
24 saturation vapor pressure at lower temperature. On the contrary, diffusion of *n*-alkanes from the surface to inner layer slowed
25 down at reduced temperature. Mechanistic studies on these processes will need to be conducted in the future to quantitatively
26 predict the influence of temperature-dependent wall-loss processes of SVOCs on laboratory experimental results.

27 **1 Introduction**

28 The environmental chamber is one of the most widely-used laboratory systems for studying chemical processes in
29 the atmosphere, including formation of secondary organic aerosol (SOA) (Clark et al., 2016; Nakao et al., 2011; Ng et al.,
30 2007; Song et al., 2005). The environmental chambers are typically made of Teflon films or stainless steel (Cocker et al., 2001;
31 Bunz et al., 1996; Voigtlaeander et al., 2012). Existence of walls in the environmental chambers induces losses of both vapors
32 and particles due to their deposition on wall surfaces (McMurry and Grosjean, 1985; Krechmer et al., 2020). Wall loss of gas-
33 phase organic compounds in the environmental chambers can lead to underestimation of SOA mass yields. For instance,
34 injection of seed particles into Teflon bag has been shown to increase SOA yields by a few times due to the reduced relative
35 importance of the chamber wall as a condensation sink in the system (Kroll et al., 2007; Zhang et al., 2014).

36 Vapor wall loss in Teflon bag chambers, especially that for semi-volatile organic compounds (SVOCs), has been
37 intensively investigated in the last decade (Matsunaga and Ziemann, 2010; Yeh and Ziemann, 2014, 2015; Zhang et al., 2015;
38 Krechmer et al., 2016; Huang et al., 2018b; Pratap et al., 2020; Yu et al., 2022). For instance, Matsunaga and Ziemann (2010)
39 studied wall-loss process of alkanes, alkenes, alcohols, and ketones. These previous wall-loss experiments were dominantly
40 conducted at around room temperature (293~303 K), as most of the chamber studies employed the corresponding temperature
41 range (Hidy, 2019). The experimental results were often modeled by assuming equilibrium dissolution of the organic
42 compounds into the Teflon film. A more recent study separately considered the surface and inner layer of the Teflon film for
43 explaining the loss process more quantitatively (Huang et al., 2018b).

44 Recently, a growing number of environmental chamber experiments have been conducted at low temperatures to
45 simulate wintertime/upper tropospheric conditions in laboratory (Huang et al., 2018a; Pratap et al., 2019; Quelever et al., 2019;
46 Simon et al., 2020; Wang et al., 2022). For instance, some SOA formation experiments have been conducted for the
47 temperature range down to 223 K using stainless steel chambers such as the Aerosol Interaction and Dynamics in the
48 Atmosphere (AIDA) and Cosmics Leaving Outdoor Droplets (CLOUD) chambers (Huang et al., 2018a; Simon et al., 2020).
49 Teflon bag chambers have also been employed for the temperature range down to 258 K (Kristensen et al., 2017; Deng et al.,
50 2021). These studies demonstrate that temperature is an important parameter determining both mass yields and chemical
51 composition of SOA. Vapor wall loss of SVOCs in the environmental chambers for the corresponding temperature range needs
52 to be understood for better interpreting these experimental data in a quantitative way. So far only one group attempted to
53 investigate vapor wall loss below room temperature, by measuring the size evolution of levoglucosan particles injected into a
54 Teflon chamber (Pratap et al., 2020). However, the experimental results were confounded by slow evaporation of levoglucosan
55 from particles at low temperatures.

56 This study investigated vapor wall loss of C₁₄-C₁₉ *n*-alkanes in a Teflon chamber for the temperature range of 262 to
57 298 K by monitoring the evolution of their gas-phase concentrations following a pulse release. The wall-loss process was

58 investigated as a function of temperature. The experimental results were analyzed using the two-layer kinetic model, which
59 considers partitioning of gas phase SVOCs to the surface layer, as well as further diffusion to the inner layer. Temperature
60 effects on the two processes were evaluated separately.

61 **2 Experimental**

62 **2.1 Teflon chamber experiments**

63 Figure 1 shows the experimental setup. The experiment was conducted using a fluorinated ethylene propylene (FEP)
64 bag with the volume of 1 m³. The thickness of the FEP film for the bag was 75 μm. The dimension of the bag was 260 cm ×
65 55 cm × 70 cm. The area to volume ratio of the chamber was 7.26 m⁻¹. The chamber volume was experimentally validated by
66 employing CO₂ as a tracer (Figure S1). The timescale for CO₂ to be well mixed in the bag after a pulse injection was
67 approximately 30 mins (Figure S1). The bag was newly purchased for the experiment, meaning that it was employed for no
68 other experiments. The bag was installed in a chest freezer (Type 2288, Nixue Inc.), which was equipped with an additional
69 internal thermal insulation layer. Two fans were installed in the freezer (outside the bag) to facilitate mixing of air so that air
70 temperature in the freezer was uniform. The temperature of the freezer was measured at 3 points using temperature sensors
71 (Figure 1). Temporal variation of temperature was ± 0.5 K at 262 K.

72 Throughout the experiments, purified air was employed. The purified air was produced using a zero air generator
73 (Model 747–30, AADCO Instruments, Inc.) and further purified using a hydrocarbon trap (BHT-2, Agilent Technologies, Inc.).
74 Hydrocarbon concentration in the purified air was less than 5 ppbv. Relative humidity (RH) was less than 0.1%.

75 Solutions containing C₁₄ - C₁₉ *n*-alkanes (Konoscience Inc., > 98%) were prepared and injected into the chamber.
76 Hexane (Fisher Chemical Co., HPLC grade) was employed as the solvent. The purities and saturation vapor pressures of all
77 chemicals are given in Table S1. The solutions were injected to the chamber using a syringe pump (Fusion 200 Touch, Chemyx
78 Inc.) and a nebulizer (TR-30-A1, Meinhard Inc.) through polytetrafluoroethylene (PTFE) tubing, as shown in Figure 1. The
79 use of nebulizer expedited the evaporation of the solution.

80 Eight sets of wall-loss experiments were conducted in the temperature range of 262 to 298 K. Prior to each experiment,
81 the chamber was heated to ~320 K and continuously flushed using purified air. The cleaning process lasted for 2~3 days until
82 the concentration of investigated *n*-alkanes dropped to the background level. To start an experiment, the chamber was switched
83 to batch mode and the solution was injected to the chamber at room temperature. The injection lasted for 13 mins, with a liquid
84 flow rate of 100 μL min⁻¹. The air flow rate of the nebulizer was 0.7 L min⁻¹. The resulting initial concentrations (*C*₀) of
85 individual *n*-alkanes in the chamber ranged from 4 to 50 μg m⁻³ assuming no wall loss, which were lower than 20% of their
86 saturation concentrations under the corresponding experimental temperature to avoid particle formation. The solution used for
87 low-temperature experiments (< 278 K) did not contain C₁₈ and C₁₉ *n*-alkanes to avoid formation of particles. For experiments

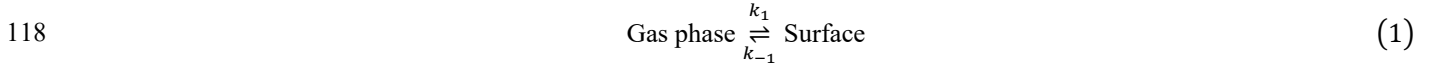
88 below room temperature, the cooling system of the freezer was turned on one hour after the completion of the injection. The
89 operation procedure was employed to avoid homogeneous nucleation and subsequent condensational growth of aerosol
90 particles. The validity of employing this post-cooled operation procedure was demonstrated by comparison with a pre-cooled
91 chamber result at 270 K (Figure S2). Measurements using an optical particle counter (11-D, GRIMM Aerosol Technik Ainring,
92 Germany) experimentally confirmed negligible abundance of aerosol particles in the chamber ($< 0.5 \mu\text{g m}^{-3}$). It took ~ 3 hours
93 for the temperature in the freezer to drop to a stable level after injection (Figure S3). Although the air in the bag leaked out
94 during experiments due to compression of the bag by its own weight, absence of intrusion of room air to the bag was confirmed
95 by observing no changes in contaminant signals (Table S2). The gas-phase concentrations of *n*-alkanes were therefore
96 unaffected by the changes in bag volume.

97 Concentrations of SVOCs in the chamber were quantified using the semi-volatile thermal desorption aerosol gas
98 chromatograph (SV-TAG, Aerodyne Research Inc. & Aerosol Dynamic Inc., USA) (Zhao et al., 2013). The gas
99 chromatography-mass spectrometer (GC-MS) (7890B, Agilent Technologies, Inc.) was employed for the system. Detailed
100 descriptions of the SV-TAG operation and performance tests were presented in our previous papers (Li et al., 2022a; Li et al.,
101 2022b). Herein, chamber air was sampled through ~ 1 m long perfluoroalkoxy alkane (PFA) tubing (1/4 inch in diameter). Prior
102 to sampling, the chamber air passed through the PFA tubing at 0.5 L min^{-1} for at least 20 min for passivating the tubing wall
103 (Matsunaga and Ziemann, 2010). Samples were periodically collected for 5 min at 4 L min^{-1} for each time at 1-15 hours after
104 injection. As the absence of particles was confirmed, only gas-phase SVOCs were sampled by the SV-TAG. The instrument
105 response to *n*-alkanes was calibrated with standards before and after each experiment (Figure S4), utilizing the in-situ automatic
106 injection system (Isaacman et al., 2011). The gas-phase concentrations of SVOCs were calculated from the measured quantity
107 of SVOCs and sampled air volume.

108 2.2 Kinetic model

109 Herein we used a unified vapor wall-loss transport model developed by Huang et al. (2018b) to fit the experimental
110 data. Figure 2 shows the concept of the model. Briefly, SVOCs partition between the gas phase and the surface of the FEP
111 film. Subsequently, the absorbed SVOCs may diffuse to the inner layer of the film. As the thickness of the FEP film ($75 \mu\text{m}$)
112 is a couple of orders larger than that of the surface layer ($\sim 5 \text{ nm}$) (Huang et al., 2018b), the inner layer is assumed as an
113 infinite sink. As a result, the diffusion process of SVOCs from the inner layer to the film surface is ignored. A list of all the
114 parameters is provided in Nomenclature. The governing equations without and with considering diffusion to the inner layer
115 are presented below, respectively.

116 (1) Without considering the diffusion process in the inner layer, the wall loss process is solely controlled by
117 partitioning of SVOCs between the gas phase and surface layer and can be described as follows



119 where k_1 and k_{-1} are forward and backward rate constants in the process. The corresponding first-order kinetic equations are

120
$$\begin{aligned} \frac{dC_{gas}}{dt} &= -k_1 C_{gas} + k_{-1} C_{surface} \\ \frac{dC_{surface}}{dt} &= k_1 C_{gas} - k_{-1} C_{surface} \end{aligned} \quad (2)$$

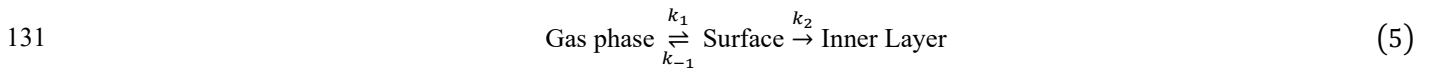
121 where C_{gas} and $C_{surface}$ are the SVOC concentrations in gas phase and on wall surface, respectively. It should be noted that
 122 $C_{surface}$ was defined as the total mass of SVOC that was divided by the chamber volume, following previous studies
 123 (Matsunaga and Ziemann, 2010; Yeh and Ziemann, 2014, 2015). This model has been commonly used to interpret the
 124 experimental data of vapor wall loss in previous studies (Matsunaga and Ziemann, 2010; Yeh and Ziemann, 2014, 2015;
 125 Zhang et al., 2015).

126 The gas-surface equilibrium time scale $\tau_{surface}$ and equilibrium constant K_{eq} can be obtained by

127
$$\tau_{surface} = \frac{1}{k_1 + k_{-1}} \quad (3)$$

128
$$K_{eq} = \frac{k_1}{k_{-1}} = \left[\frac{C_{surface}}{C_{gas}} \right]_{eq} \quad (4)$$

129 (2) Considering the diffusion process in the inner layer, the whole vapor wall loss process can be formulated as
 130 follows



132 where k_2 is the first-order loss rate constant in the diffusion process. Correspondingly, the kinetic processes for C_{gas} and
 133 $C_{surface}$ can be described by the following equations

134
$$\begin{aligned} \frac{dC_{gas}}{dt} &= -k_1 C_{gas} + k_{-1} C_{surface} \\ \frac{dC_{surface}}{dt} &= k_1 C_{gas} - k_{-1} C_{surface} - k_2 C_{surface} \end{aligned} \quad (6)$$

135 The diffusion process has the first-order decay time scale τ_{inner} of $\tau_{inner} = \frac{1}{k_2}$. If $k_2 \ll k_1 + k_{-1}$ (*i.e.*, $\tau_{inner} \gg \tau_{surface}$),
136 gas-surface partitioning occurs much faster than the diffusion process to the inner layer. In this case, the apparent first-order
137 decay loss constant of SVOC from the gas phase can asymptotically be represented as (Huang et al., 2018b):

$$138 \quad \frac{dC_{gas}}{C_{gas}dt} \approx -\frac{K_{eq}}{1 + K_{eq}}k_2 \quad (7)$$

139 The data analysis and model fitting were conducted using Wolfram Mathematica 13.1. The controlling factors of
140 individual parameters in the above equations were previously discussed by Huang et al. (2018b).

141 **3 Results and discussion**

142 **3.1 Wall loss of *n*-alkanes at room temperature**

143 An example of temporal profile for C₁₄-C₁₉ *n*-alkanes during the experiment at 298 K is shown in Figure 3. The figure
144 demonstrates the temporal change of C_{gas}/C_0 , where C_0 indicates the initial concentration of *n*-alkanes. The values of C_{gas}/C_0
145 for each *n*-alkane exhibited similar patterns. During the first one hour following the injection, C_{gas}/C_0 exponentially decreased.
146 After that, gradual decreases in C_{gas}/C_0 were observed. For example, the decline in gas fraction for C₁₄ *n*-alkane during the
147 first hour accounted for 71% of the total change in C_{gas}/C_0 over the whole experimental period of 15 hours. The values of
148 C_{gas}/C_0 decreased with the increase in carbon number, indicating enhanced wall loss. The values of C_{gas}/C_0 at 15 hours after
149 injection were 0.32, 0.25, 0.16, 0.097, 0.069, and 0.037 for C₁₄ - C₁₉ *n*-alkanes, respectively.

150 The experimental result can be well fitted using the two-layer model, but the fits deteriorate in the case that diffusion
151 in the inner layer is neglected (Figure 3). The optimized parameter sets are shown in Table S3. Mass fractions of injected
152 chemical species in the gas, surface, and inner layer phases that were estimated using the model are shown in Figure S5. In the
153 case of the most volatile compound (C₁₄ *n*-alkane), the maximum mass fraction in the surface phase occurred at 2 hours after
154 injection. Subsequently, the mass fractions for the compound in both gas phase and surface layer gradually decreased. During
155 this period, the ratio of the mass in the surface layer to that in the gas phase stabilized at 1.33. The mass fraction of the
156 compound in the inner layer steadily increased, reaching 0.22 at 15 hours after injection.

157 In the case of the least volatile compound (C₁₉ *n*-alkane), the mass fraction in the surface layer reached the maximum
158 (~76%) approximately 1 hour after injection, accounting for the rapid decrease in the observed concentration in the gas phase.
159 Subsequently, mass fractions of the compound in the gas phase and in the surface layer decreased in proportion. The
160 concentration ratio of the gas phase and surface later was maintained as a constant (Figure S5). The mass fraction of the

161 compound in the inner layer kept increasing during the experiment. At 15 hours after injection, 87% of the compound existed
162 in the inner layer.

163 The time scale for *n*-alkanes to reach partitioning equilibrium between the gas and surface phases is estimated to be
164 12 ~ 35 mins, consistent with literature data. For example, Matsunaga and Ziemann (2010) reported that the corresponding
165 time scale for C₈ - C₁₆ alkanes was 60 ± 20 mins. The corresponding value for oxygenated organic compounds was reported
166 as 26 ± 23 mins (Yeh and Ziemann, 2015).

167 Our result for the mass transfer of SVOCs to the inner layer can also be compared with a previous study. The rates
168 for the decrease in C_{gas}/C_0 for C₁₄-C₁₉ *n*-alkanes were 0.6–1.3% hour⁻¹ after the partitioning between gas phase and surface
169 layer reached equilibrium (*i.e.*, 3 ~ 15 hours). Yeh and Ziemann (2015) reported the corresponding value for 2-ketones as
170 approximately 1% hour⁻¹ for the time scale of 7 hours. They suggested that the value is close to the theoretical value for the
171 Fickian diffusion loss rate (~0.5 % hour⁻¹).

172 3.2 Temperature dependence of wall loss of *n*-alkanes

173 Figure 4a summarizes the values of C_{gas}/C_0 for all experiments at 3 hours after injection. The data for this sampling
174 time was selected, as the loss of gas phase species by partitioning to the surface layer accounted for the dominant portion of
175 the decline in the gas phase concentration. It should be noted that fitting the experimental data using the two-layer model was
176 challenging for the low-temperature experiments. Since the chamber was cooled after the injection of *n*-alkanes, the model
177 parameters would change correspondingly with chamber temperature. Potential uncertainties associated with the employment
178 of the data at 3 hours after injection as a proxy for gas-surface partitioning are summarized in Text S1.

179 Generally, C_{gas}/C_0 was lower for less volatile compounds and at lower temperature, suggesting enhanced partitioning
180 of *n*-alkanes to the chamber wall. The data for the room temperature ($C_{gas}/C_0 = 0.47, 0.45, 0.34, 0.24, 0.17,$ and 0.091 for C₁₄,
181 C₁₅, C₁₆, C₁₇, C₁₈, and C₁₉ *n*-alkanes) were smaller than that have been reported by a previous study. Namely, Matsunaga and
182 Ziemann (2010) quantified the corresponding values for equilibration between the gas and surface phases for C₁₄-C₁₆ *n*-alkanes
183 as ~80 – 90%. The enhanced partitioning to the surface layer in our study is likely due to that the chamber for the present study
184 has a larger area to volume ratio (7.26 m⁻¹ versus 3.39 m⁻¹).

185 Figure 4b shows the values of C_{gas}/C_0 as a function of temperature at 15 hours after injection. In all experiments, the
186 values of C_{gas}/C_0 at 15 hours after injection were consistently lower than those for 3 hours. For instance, C_{gas}/C_0 for C₁₄ *n*-
187 alkane at 262 K decreased from 0.15 (3 hours) to 0.06 (15 hours). As discussed in the case of the experiment at 298 K, the
188 result suggests that diffusional loss in the inner layer of the chamber wall occurred for the whole temperature range.

189 3.3 Temperature dependence of partitioning between gas phase and wall surface

190 The temperature dependence in the data summarized in Figure 4a can be understood by considering changes in
191 partitioning between the gas phase and surface layer. Matsunaga and Ziemann (2010) introduced the following equation for
192 relating $C_{surface}/C_{gas}$ and temperature based on the equilibrium dissolution model:

$$193 \left[\frac{C_{surface}}{C_{gas}} \right]_{eq} = K_{eq} = \frac{C_{FEP_surface}RT}{M_{wall}\gamma_{FEP_surface}P_s(T)} \quad (8)$$

194 where $C_{FEP_surface}$ is the equivalent organic mass concentration of the FEP chamber surface wall, M_{wall} is the average
195 molecular mass of the FEP, $\gamma_{FEP_surface}$ is the activity coefficient of the organic compound in the Teflon surface, R is the gas
196 constant, and T is temperature. $P_s(T)$ is the saturation vapor pressure of the compound at temperature T . To use Equation (8)
197 $P_s(T)$ was calculated by the EVAPORATION group contribution method (Compernelle et al., 2011). Comparison between
198 the EVAPORATION method with other approaches for estimating $P_s(T)$ is available in Figure S6. The value of
199 $[C_{surface}/C_{gas}]_{eq}$ was approximated using $1/[C_{gas}/C_0]_{at\ 3\ hours} - 1$ by assuming that diffusion of n -alkanes to the inner layer
200 was still a minor loss process within 3 hours. Among the terms for the right-hand-side of equation (8), $RT/P_s(T)$ can be
201 calculated from the experimental conditions. The equation suggests that $[C_{surface}/C_{gas}]_{eq}$ and $RT/P_s(T)$ may linearly
202 correlate with the slope of $C_{FEP_surface}/(M_{wall}\gamma_{FEP_surface})$.

203 Figure 5 shows the correlations between $C_{surface}/C_{gas}$ and $RT/P_s(T)$ for individual compounds. For all the tested
204 compounds, these two parameters correlated well, even though $C_{surface}/C_{gas}$ increased by more than one order of magnitude
205 when the chamber was cooled down. The result suggests that equation (8) can be applied to a wide range of temperatures
206 without considering the temperature dependence of $C_{FEP_surface}/(M_{wall}\gamma_{FEP_surface})$ to account for partitioning of n -alkanes
207 to the surface layer. In other word, $\gamma_{FEP_surface}$ can be practically treated as a constant for the investigated temperature range,
208 given $C_{FEP_surface}$ and M_{wall} are independent of temperature. This implication is consistent with previous findings that the
209 activity coefficients of organic compounds in polymers only change slightly with temperature. For instance, Kontogeorgis et
210 al. (1993) compared the experimental and modelled values of activity coefficients for hydrocarbons in a few polymers such as
211 low-density polyethylene. The values of activity coefficients change by 10~20% for a temperature change of 100 K. Further
212 studies, that employ different chemical species, would be needed in the future for validating and applying the relation to a
213 wider range.

214 Values of $\gamma_{FEP_surface}$ for n -alkanes can be estimated from Figure 5. Based on equation (8), the fitted slopes
215 correspond to $C_{FEP_surface}/(M_{wall}\gamma_{FEP_surface})$. For a specific chamber design, compound-independent $C_{FEP_surface}$ can be
216 estimated by the density of FEP film (2150 kg m^{-3}) and the thickness of surface layer ($\sim 5\text{ nm}$) (Huang et al., 2018b). For the

217 chamber in this experiment, $C_{FEP_surface}$ was assumed as 78.2 mg m^{-3} , following the recommendation by Huang et al. (2018b).
218 For estimating compound-dependent $\gamma_{FEP_surface}$, previous studies assumed $M_{wall} = 200 \text{ g mol}^{-1}$ (Huang et al., 2018b;
219 Matsunaga and Ziemann, 2010). The same approximations were employed in the present study.

220 Figure 6 plots the retrieved values of $\gamma_{FEP_surface}$ for *n*-alkanes against $P_s(298 \text{ K})$ for *n*-alkanes. The figure also
221 shows the corresponding parameters obtained from previous experimental studies (compiled by Huang et al. (2018b), including
222 Matsunaga and Ziemann (2010), Yeh and Ziemann (2014, 2015), and Krechmer et al. (2016)). It should be noted that the
223 literature results were analyzed with fixed values of area to volume ratio of 3 m^{-1} and $C_{FEP_surface}$ of 32.2 mg m^{-3} (Huang et
224 al., 2018b). Regardless of differences in types of chemicals and chambers, the experimentally estimated values of $\gamma_{FEP_surface}$
225 and $P_s(298 \text{ K})$ correlate in logarithmic scale. The relationship followed the equation of $\ln(\gamma_{FEP_surface}) = 0.40 -$
226 $0.61\ln(P_s(298 \text{ K}))$.

227 3.4 Characterization of diffusion from the Teflon surface to inner layer

228 Values of k_2 were estimated using equation (7), since values of τ_{inner} are at least 18 times larger than those of
229 $\tau_{surface}$ (Table S3). The values of C_{gas}/C_0 at 3 hours after injection were employed to calculate K_{eq} as discussed earlier.
230 The experimental data for 9, 12, and 15 hours after injection was employed for obtaining k_2 .

231 Figure 7 plots the estimated values of k_2 against $P_s(T)$ for all compounds in all experiments. The values of k_2 and
232 $P_s(T)$ positively correlate. As a comparison point, a previous study reported positive correlations for (1) the diffusivity of
233 organic compounds in FEP film and saturation concentration, and (2) k_2 and diffusivity (Huang et al., 2018b). Our current
234 result is qualitatively similar to the previous study, though temperature was maintained as a constant in the previous study.
235 The decrease in k_2 at lower temperature could be induced by reduced viscosity in the inner layer or weakened thermal motion
236 of *n*-alkane molecules (Mattila et al., 2023). It should be noted that compression of bag volume during experiment would lead
237 to an increase in the area to volume ratio. Consequently, this could disrupt the relatively slow diffusion process. Based on
238 some photos during the experiment, the leak-out air could have increased the area to volume ratio by a few factors. Further
239 study, that incorporates considering changes of chamber volume, would be needed in the future for quantitatively interpreting
240 the data.

241 4 Conclusions

242 The present study investigated the wall loss process of C_{14} - C_{19} *n*-alkanes to the wall of a 1 m^3 chamber bag, which was
243 composed of FEP film. The temperature of the chamber was controlled for the range of 262 to 298 K. Decay in gas-phase
244 concentrations of the *n*-alkanes was quantified using the SV-TAG for 15 hours following injection. The temporal variations in
245 the *n*-alkane concentrations suggested two types of loss processes. The first process was characterized by rapid exponential

246 decay in the first few hours. Subsequently, slow first-order decreases in the *n*-alkane concentrations were identified until the
247 end of the experiment. Enhanced wall loss was observed at lower temperatures for all compounds.

248 The experimental data were well fitted using the two-layer kinetic model, which considers partitioning of gas-phase
249 species to the surface layer of the chamber film and further diffusion to the inner layer. The analysis suggests that when the
250 Teflon bag chamber is operated at low temperatures, partitioning of gas phase species to the chamber wall surface is enhanced,
251 whereas the permeation of the chemical compounds to the inner layer is suppressed. The temperature effect on gas-surface
252 partitioning overweighs that on diffusion into the inner layer for *n*-alkanes, leading to an overall enhanced wall loss at lower
253 temperature.

254 The quasi-equilibrium partitioning of *n*-alkanes between the gas phase and surface layer was interpreted by considering
255 the dissolution process of the species into the surface layer. Values of $C_{surface}/C_{gas}$ at quasi-equilibrium are proportional to
256 $RT/P_s(T)$ for individual compounds. The result suggests that decreased saturation vapor pressure is the major driving force
257 for enhanced partitioning to the surface layer at low temperatures for all investigated compounds, while their activity
258 coefficients can be practically treated as constants for the investigated temperature range. The relationship can be potentially
259 employed for predicting changes in wall loss of SVOCs as a function of temperature, after further verification employing other
260 types of organic compounds.

261 In the future, the underlying mechanisms of the present findings will need to be sought for a better understanding of the
262 chamber wall loss of SVOCs. The present study focused on *n*-alkanes. In the case of chamber experiments for SOA formation,
263 wall loss processes of oxygenated chemical species would be more important. Thus, a temperature-dependent wall loss study
264 for oxygenated chemical species will still need to be conducted for interpreting SOA chamber experiments under a wide range
265 of temperatures.

266 **Data Availability**

267 Data will be made available on request.

268 **Author contribution**

269 **Longkun He:** Conceptualization, Methodology, Experiment, Data curation, Formal analysis, Writing – original draft. **Wenli**
270 **Liu:** Methodology, Experiment, Writing – review & editing. **Yatai Li:** Methodology, Writing – review & editing. **Jixuan**
271 **Wang:** Experiment, Writing – review & editing. **Mikinori Kuwata:** Conceptualization, Methodology, Project administration,
272 Funding acquisition, Formal analysis, Writing – review & editing, Supervision. **Yingjun Liu:** Conceptualization,
273 Methodology, Project administration, Funding acquisition, Formal analysis, Writing – review & editing, Supervision.

274 **Competing interests**

275 The authors declare that they have no conflict of interest.

276 **Acknowledgements**

277 We thank Dr. Ying Zhou for assisting to improve figure quality. This research was supported by the National Natural

278 Science Foundation of China (92044303, 42175121, and 42150610485).

279 **Reference**

280 Bunz, H., Möhler, O., Naumann, K., Saathoff, H., Schöck, W., and Schurath, U.: The novel aerosol chamber facility
281 AIDA: status and first results, Proc. 7th European Symposium on the Physico-Chemical Behaviour of Atmospheric Pollutants,
282 1996.

283 Clark, C. H., Kacarab, M., Nakao, S., Asa-Awuku, A., Sato, K., and Cocker, D. R., III: Temperature Effects on Secondary
284 Organic Aerosol (SOA) from the Dark Ozonolysis and Photo-Oxidation of Isoprene, Environ. Sci. Technol., 50, 5564-5571,
285 <https://doi.org/10.1021/acs.est.5b05524>, 2016.

286 Cocker, D. R., Flagan, R. C., and Seinfeld, J. H.: State-of-the-art chamber facility for studying atmospheric aerosol
287 chemistry, Environ. Sci. Technol., 35, 2594-2601, <https://doi.org/10.1021/es0019169>, 2001.

288 Compernelle, S., Ceulemans, K., and Muller, J. F.: EVAPORATION: a new vapour pressure estimation method for
289 organic molecules including non-additivity and intramolecular interactions, Atmos. Chem. Phys., 11, 9431-9450,
290 <https://doi.org/10.5194/acp-11-9431-2011>, 2011.

291 Deng, Y. G., Inomata, S., Sato, K., Ramasamy, S., Morino, Y., Enami, S., and Tanimoto, H.: Temperature and acidity
292 dependence of secondary organic aerosol formation from alpha-pinene ozonolysis with a compact chamber system, Atmos.
293 Chem. Phys., 21, 5983-6003, <https://doi.org/10.5194/acp-21-5983-2021>, 2021.

294 Hidy, G. M.: Atmospheric Chemistry in a Box or a Bag, Atmosphere, 10, <https://doi.org/10.3390/atmos10070401>, 2019.

295 Huang, W., Saathoff, H., Pajunoja, A., Shen, X. L., Naumann, K. H., Wagner, R., Virtanen, A., Leisner, T., and Mohr,
296 C.: alpha-Pinene secondary organic aerosol at low temperature: chemical composition and implications for particle viscosity,
297 Atmos. Chem. Phys., 18, 2883-2898, <https://doi.org/10.5194/acp-18-2883-2018>, 2018a.

298 Huang, Y. L., Zhao, R., Charan, S. M., Kenseth, C. M., Zhang, X., and Seinfeld, J. H.: Unified Theory of Vapor-Wall
299 Mass Transport in Teflon-Walled Environmental Chambers, Environ. Sci. Technol., 52, 2134-2142,
300 <https://doi.org/10.1021/acs.est.7b05575>, 2018b.

301 Isaacman, G., Kreisberg, N. M., Worton, D. R., Hering, S. V., and Goldstein, A. H.: A versatile and reproducible
302 automatic injection system for liquid standard introduction: application to in-situ calibration, Atmos. Meas. Tech., 4, 1937-
303 1942, <https://doi.org/10.5194/amt-4-1937-2011>, 2011.

304 Kontogeorgis, G. M., Fredenslund, A., and Tassios, D. P.: Simple Activity-Coefficient Model for The Prediction of
305 Solvent Activities in Polymer-Solutions, Ind. Eng. Chem. Res., 32, 362-372, <https://doi.org/10.1021/ie00014a013>, 1993.

306 Krechmer, J. E., Day, D. A., and Jimenez, J. L.: Always Lost but Never Forgotten: Gas-Phase Wall Losses Are Important
307 in All Teflon Environmental Chambers, Environ. Sci. Technol., 54, 12890-12897, <https://doi.org/10.1021/acs.est.0c03381>,
308 2020.

309 Krechmer, J. E., Pagonis, D., Ziemann, P. J., and Jimenez, J. L.: Quantification of Gas-Wall Partitioning in Teflon
310 Environmental Chambers Using Rapid Bursts of Low-Volatility Oxidized Species Generated in Situ, Environ. Sci. Technol.,
311 50, 5757-5765, <https://doi.org/10.1021/acs.est.6b00606>, 2016.

312 Kristensen, K., Jensen, L. N., Glasius, M., and Bilde, M.: The effect of sub-zero temperature on the formation and
313 composition of secondary organic aerosol from ozonolysis of alpha-pinene, *Environ. Sci.-Process Impacts*, 19, 1220-1234,
314 <https://doi.org/10.1039/c7em00231a>, 2017.

315 Kroll, J. H., Chan, A. W. H., Ng, N. L., Flagan, R. C., and Seinfeld, J. H.: Reactions of semivolatile organics and their
316 effects on secondary organic aerosol formation, *Environ. Sci. Technol.*, 41, 3545-3550, <https://doi.org/10.1021/es062059x>,
317 2007.

318 Li, Y. T., He, L. K., Xie, D., Zhao, A. Q., Wang, L. X., Kreisberg, N. M., Jayne, J., and Liu, Y. J.: Strong temperature
319 influence and indiscernible ventilation effect on dynamics of some semivolatile organic compounds in the indoor air of an
320 office, *Environ. Int.*, 165, <https://doi.org/10.1016/j.envint.2022.107305>, 2022a.

321 Li, Y. T., Xie, D., He, L. K., Zhao, A. Q., Wang, L. X., Kreisberg, N. M., Jayne, J., and Liu, Y. J.: Dynamics of di-2-
322 ethylhexyl phthalate (DEHP) in the indoor air of an office, *Build. Environ.*, 223,
323 <https://doi.org/10.1016/j.buildenv.2022.109446>, 2022b.

324 Matsunaga, A. and Ziemann, P. J.: Gas-Wall Partitioning of Organic Compounds in a Teflon Film Chamber and Potential
325 Effects on Reaction Product and Aerosol Yield Measurements, *Aerosol Sci. Technol.*, 44, 881-892,
326 <https://doi.org/10.1080/02786826.2010.501044>, 2010.

327 Mattila, J. M., Li, E. Y., and Offenberg, J. H.: Tubing material considerably affects measurement delays of gas-phase
328 oxygenated per- and polyfluoroalkyl substances, *J. Air Waste Manage. Assoc.*, 73, 335-344,
329 <https://doi.org/10.1080/10962247.2023.2174612>, 2023.

330 McMurry, P. H. and Grosjean, D.: Gas and Aerosol Wall Losses in Teflon Film Smog Chambers, *Environ. Sci. Technol.*,
331 19, 1176-1182, <https://doi.org/10.1021/es00142a006>, 1985.

332 Nakao, S., Shrivastava, M., Anh, N., Jung, H., and Cocker, D., III: Interpretation of Secondary Organic Aerosol Formation
333 from Diesel Exhaust Photooxidation in an Environmental Chamber, *Aerosol Sci. Technol.*, 45,
334 <https://doi.org/10.1080/02786826.2011.573510>, 2011.

335 Ng, N. L., Chhabra, P. S., Chan, A. W. H., Surratt, J. D., Kroll, J. H., Kwan, A. J., McCabe, D. C., Wennberg, P. O.,
336 Sorooshian, A., Murphy, S. M., Dalleska, N. F., Flagan, R. C., and Seinfeld, J. H.: Effect of NO_x level on secondary organic
337 aerosol (SOA) formation from the photooxidation of terpenes, *Atmos. Chem. Phys.*, 7, 5159-5174, [https://doi.org/10.5194/acp-](https://doi.org/10.5194/acp-7-5159-2007)
338 [7-5159-2007](https://doi.org/10.5194/acp-7-5159-2007), 2007.

339 Pratap, V., Bian, Q. J., Kiran, S. A., Hopke, P. K., Pierce, J. R., and Nakao, S.: Investigation of levoglucosan decay in
340 wood smoke smog-chamber experiments: The importance of aerosol loading, temperature, and vapor wall losses in interpreting
341 results, *Atmos. Environ.*, 199, 224-232, <https://doi.org/10.1016/j.atmosenv.2018.11.020>, 2019.

342 Pratap, V., Kiran, S. A., Bian, Q., Pierce, J. R., Hopke, P. K., and Nakao, S.: Observation of Vapor Wall Deposition in a
343 Smog Chamber Using Size Evolution of Pure Organic Particles, *Aerosol Air Qual. Res.*, 20, 2705-2714,
344 <https://doi.org/10.4209/aaqr.2020.05.0268>, 2020.

345 Quelever, L. L. J., Kristensen, K., Jensen, L. N., Rosati, B., Teiwes, R., Daellenbach, K. R., Perakyla, O., Roldin, P.,
346 Bossi, R., Pedersen, H. B., Glasius, M., Bilde, M., and Ehn, M.: Effect of temperature on the formation of highly oxygenated
347 organic molecules (HOMs) from alpha-pinene ozonolysis, *Atmos. Chem. Phys.*, 19, 7609-7625, [https://doi.org/10.5194/acp-](https://doi.org/10.5194/acp-19-7609-2019)
348 [19-7609-2019](https://doi.org/10.5194/acp-19-7609-2019), 2019.

349 Simon, M., Dada, L., Heinritzi, M., Scholz, W., Stolzenburg, D., Fischer, L., Wagner, A. C., Kurten, A., Rorup, B., He, X. C.,
350 Almeida, J., Baalbaki, R., Baccharini, A., Bauer, P. S., Beck, L., Bergen, A., Bianchi, F., Brakling, S., Brilke, S., Caudillo,
351 L., Chen, D. X., Chu, B. W., Dias, A., Draper, D. C., Duplissy, J., El-Haddad, I., Finkenzeller, H., Frege, C., Gonzalez-
352 Carracedo, L., Gordon, H., Granzin, M., Hakala, J., Hofbauer, V., Hoyle, C. R., Kim, C., Kong, W. M., Lamkaddam, H.,
353 Lee, C. P., Lehtipalo, K., Leiminger, M., Mai, H. J., Manninen, H. E., Marie, G., Marten, R., Mentler, B., Molteni, U.,
354 Nichman, L., Nie, W., Ojdanic, A., Onnela, A., Partoll, E., Petaja, T., Pfeifer, J., Philippov, M., Quelever, L. L. J.,
355 Ranjithkumar, A., Rissanen, M. P., Schallhart, S., Schobesberger, S., Schuchmann, S., Shen, J. L., Sipila, M., Steiner, G.,
356 Stozhkov, Y., Tauber, C., Tham, Y. J., Tome, A. R., Vazquez-Pufleau, M., Vogel, A. L., Wagner, R., Wang, M. Y., Wang,
357 D. S., Wang, Y. H., Weber, S. K., Wu, Y. S., Xiao, M., Yan, C., Ye, P. L., Ye, Q., Zauner-Wieczorek, M., Zhou, X. Q.,
358 Baltensperger, U., Dommen, J., Flagan, R. C., Hansel, A., Kulmala, M., Volkamer, R., Winkler, P. M., Worsnop, D. R.,
359 Donahue, N. M., Kirkby, J., and Curtius, J.: Molecular understanding of new-particle formation from alpha-pinene
360 between-50 and+25 degrees C, *Atmos. Chem. Phys.*, 20, 9183-9207, <https://doi.org/10.5194/acp-20-9183-2020>, 2020.

361 Song, C., Na, K. S., and Cocker, D. R.: Impact of the hydrocarbon to NOx ratio on secondary organic aerosol formation,
362 *Environ. Sci. Technol.*, 39, 3143-3149, <https://doi.org/10.1021/es0493244>, 2005.

363 Voigtlaeander, J., Duplissy, J., Rondo, L., Kuerten, A., and Stratmann, F.: Numerical simulations of mixing conditions
364 and aerosol dynamics in the CERN CLOUD chamber, *Atmos. Chem. Phys.*, 12, 2205-2214, [https://doi.org/10.5194/acp-12-](https://doi.org/10.5194/acp-12-2205-2012)
365 [2205-2012](https://doi.org/10.5194/acp-12-2205-2012), 2012.

366 Wang, M. Y., Xiao, M., Bertozzi, B., Marie, G., Rorup, B., Schulze, B., Bardakov, R., He, X. C., Shen, J. L., Scholz, W.,
367 Marten, R., Dada, L., Baalbaki, R., Lopez, B., Lamkaddam, H., Manninen, H. E., Amorim, A., Ataei, F., Bogert, P., Brasseur,
368 Z., Caudillo, L., De Menezes, L. P., Duplissy, J., Ekman, A. M. L., Finkenzeller, H., Carracedo, L. G., Granzin, M., Guida, R.,
369 Heinritzi, M., Hofbauer, V., Hohler, K., Korhonen, K., Krechmer, J. E., Kurten, A., Lehtipalo, K., Mahfouz, N. G. A.,
370 Makhmutov, V., Massabo, D., Mathot, S., Mauldin, R. L., Mentler, B., Muller, T., Onnela, A., Petaja, T., Philippov, M.,
371 Piedehierro, A. A., Pozzer, A., Ranjithkumar, A., Schervish, M., Schobesberger, S., Simon, M., Stozhkov, Y., Tome, A., Umo,
372 N. S., Vogel, F., Wagner, R., Wang, D. S., Weber, S. K., Welti, A., Wu, Y. S., Zauner-Wieczorek, M., Sipila, M., Winkler, P.
373 M., Hansel, A., Baltensperger, U., Kulmala, M., Flagan, R. C., Curtius, J., Riipinen, I., Gordon, H., Lelieveld, J., El-Haddad,
374 I., Volkamer, R., Worsnop, D. R., Christoudias, T., Kirkby, J., Mohler, O., and Donahue, N. M.: Synergistic HNO3-H2SO4-
375 NH3 upper tropospheric particle formation, *Nature*, 605, 483-+, <https://doi.org/10.1038/s41586-022-04605-4>, 2022.

376 Yeh, G. K. and Ziemann, P. J.: Alkyl Nitrate Formation from the Reactions of C-8-C-14 n-Alkanes with OH Radicals in
377 the Presence of NOx: Measured Yields with Essential Corrections for Gas-Wall Partitioning, *J. Phys. Chem. A*, 118, 8147-
378 8157, <https://doi.org/10.1021/jp500631v>, 2014.

379 Yeh, G. K. and Ziemann, P. J.: Gas-Wall Partitioning of Oxygenated Organic Compounds: Measurements, Structure-
380 Activity Relationships, and Correlation with Gas Chromatographic Retention Factor, *Aerosol Sci. Technol.*, 49, 726-737,
381 <https://doi.org/10.1080/02786826.2015.1068427>, 2015.

382 Yu, S., Jia, L., Xu, Y., Zhang, H., Zhang, Q., and Pan, Y.: Wall losses of oxygenated volatile organic compounds from
383 oxidation of toluene: Effects of chamber volume and relative humidity *, *J. Environ. Sci.*, 114, 475-484,
384 <https://doi.org/10.1016/j.jes.2021.09.026>, 2022.

385 Zhang, X., Cappa, C. D., Jathar, S. H., McVay, R. C., Ensberg, J. J., Kleeman, M. J., and Seinfeld, J. H.: Influence of
386 vapor wall loss in laboratory chambers on yields of secondary organic aerosol, *Proc. Natl. Acad. Sci. U. S. A.*, 111, 5802-5807,
387 <https://doi.org/10.1073/pnas.1404727111>, 2014.

388 Zhang, X., Schwantes, R. H., McVay, R. C., Lignell, H., Coggon, M. M., Flagan, R. C., and Seinfeld, J. H.: Vapor wall
389 deposition in Teflon chambers, *Atmos. Chem. Phys.*, 15, 4197-4214, <https://doi.org/10.5194/acp-15-4197-2015>, 2015.

390 Zhao, Y. L., Kreisberg, N. M., Worton, D. R., Teng, A. P., Hering, S. V., and Goldstein, A. H.: Development of an In
391 Situ Thermal Desorption Gas Chromatography Instrument for Quantifying Atmospheric Semi-Volatile Organic Compounds,
392 *Aerosol Sci. Technol.*, 47, 258-266, <https://doi.org/10.1080/02786826.2012.747673>, 2013.

393 **Nomenclature**

394 A table that contains the definitions of parameters and corresponding units.

395 k_1 forward rate constant (s^{-1})

396 k_{-1} backward rate constant (s^{-1})

397 k_2 first-order loss rate constant (s^{-1})

398 $\tau_{surface}$ gas-surface equilibrium time scale (min)

399 τ_{inner} diffusion time scale (min)

400 C_0 initial SVOC concentration in gas phase ($\mu g\ m^{-3}$)

401 C_{gas} SVOC concentration in gas phase ($\mu g\ m^{-3}$)

402 C_{wall} SVOC concentration on wall surface ($\mu g\ m^{-3}$)

403 K_{eq} gas-surface equilibrium constant

404 $C_{FEP_surface}$ equivalent organic mass concentration of the FEP chamber surface ($mg\ m^{-3}$)

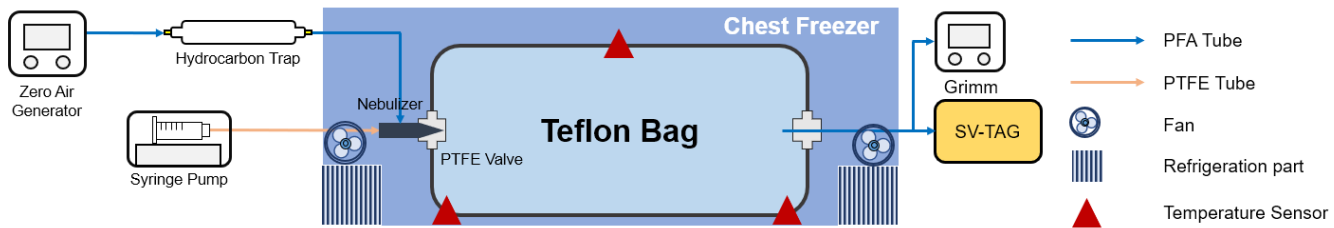
405 M_{wall} average molecular mass of the Teflon wall ($g\ mol^{-1}$)

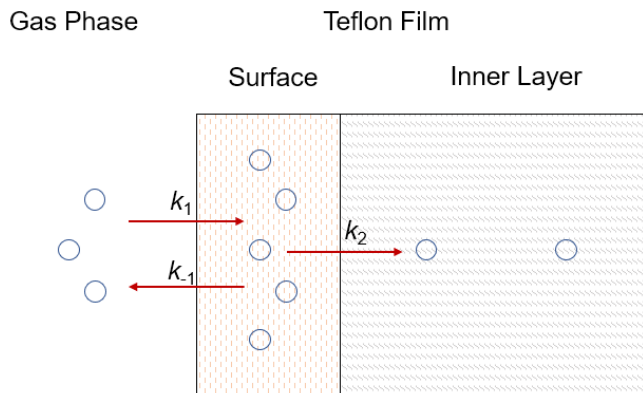
406 $\gamma_{FEP_surface}$ activity coefficient in the Teflon surface

407 R gas constant ($J\ K^{-1}\ mol^{-1}$)

408 T temperature (K)

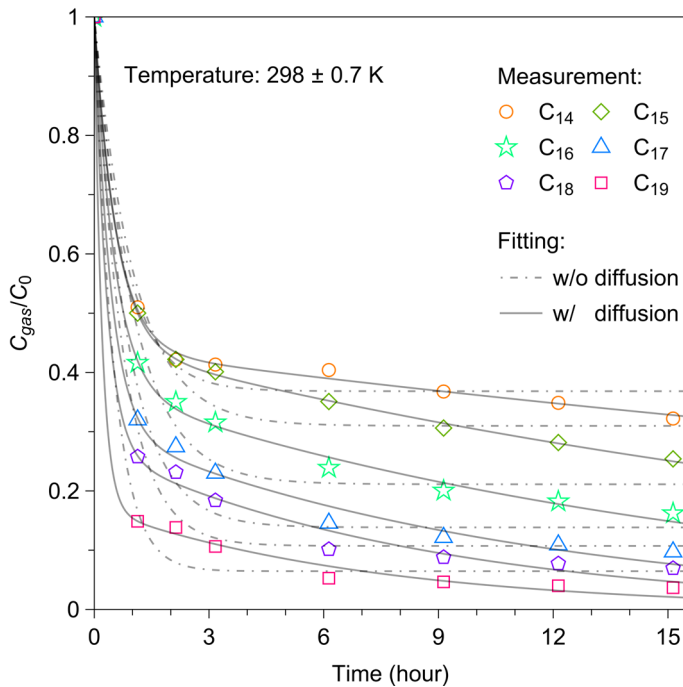
409 $P_s(T)$ saturation vapor pressure of compound at temperature T (Pa)





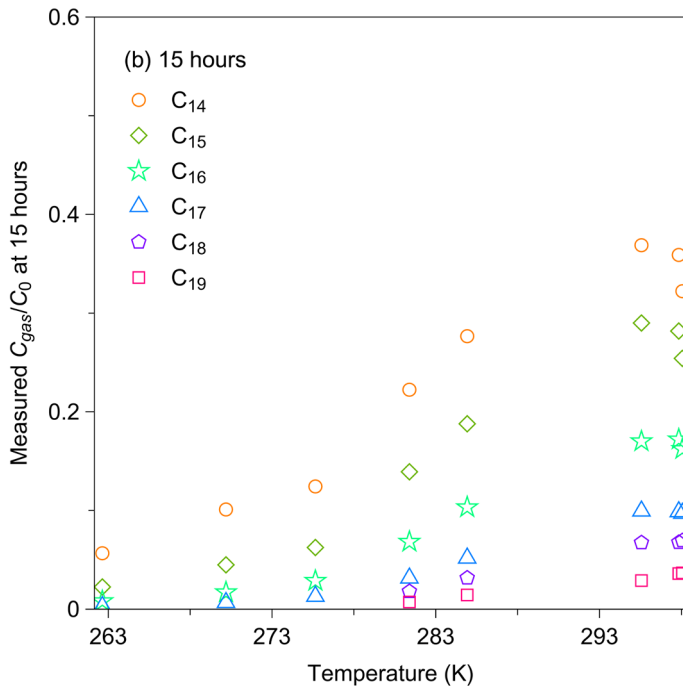
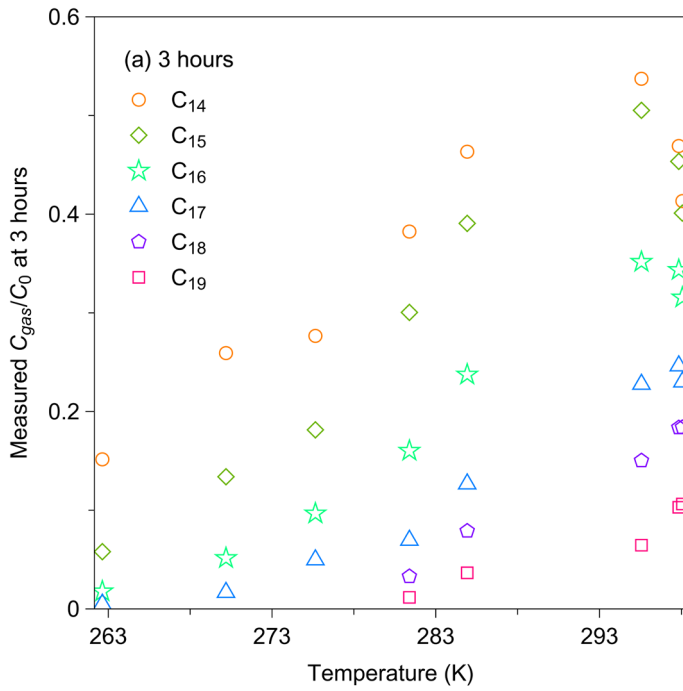
412

413 **Figure 2.** Schematic diagram of wall loss process. Compounds partition between gas phase and surface layer with forward
414 and backward rates (k_1 and k_{-1}). Compounds in surface layer undergo irreversible diffusion into inner layer with first-order
415 loss rate (k_2).



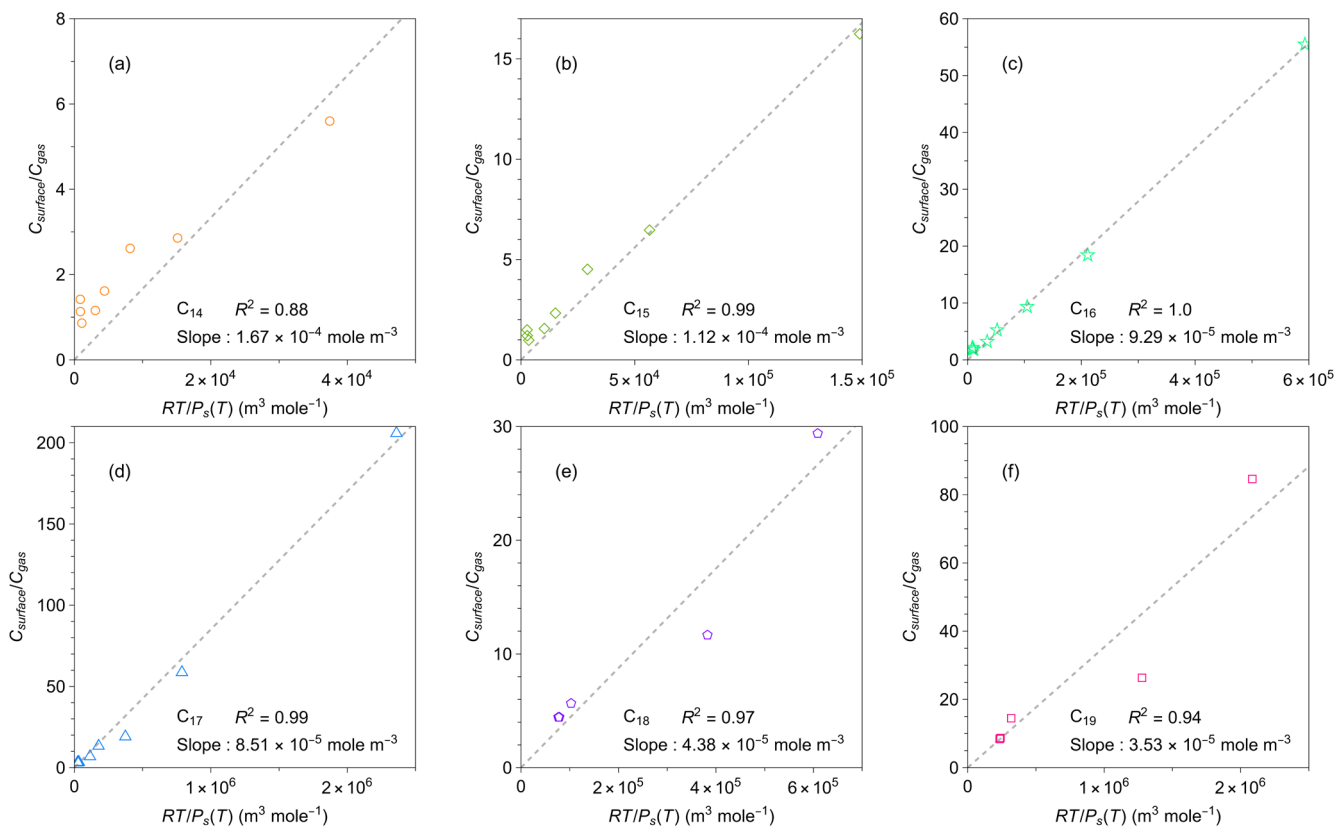
416

417 **Figure 3.** Temporal variation in C_{gas}/C_0 for C₁₄-C₁₉ *n*-alkanes at 298 ± 0.7 K following injection. C_{gas} is the concentration of
 418 each *n*-alkane in the gas phase, and C_0 is the corresponding initial concentration of each *n*-alkane. The two-layer kinetic
 419 sorption model (Section 2.2) was employed to fit the data (black solid line). The black dot-dashed lines show the fitting result
 420 to the model that ignores the diffusion process to the inner layer (*i.e.*, $k_2 = 0$).



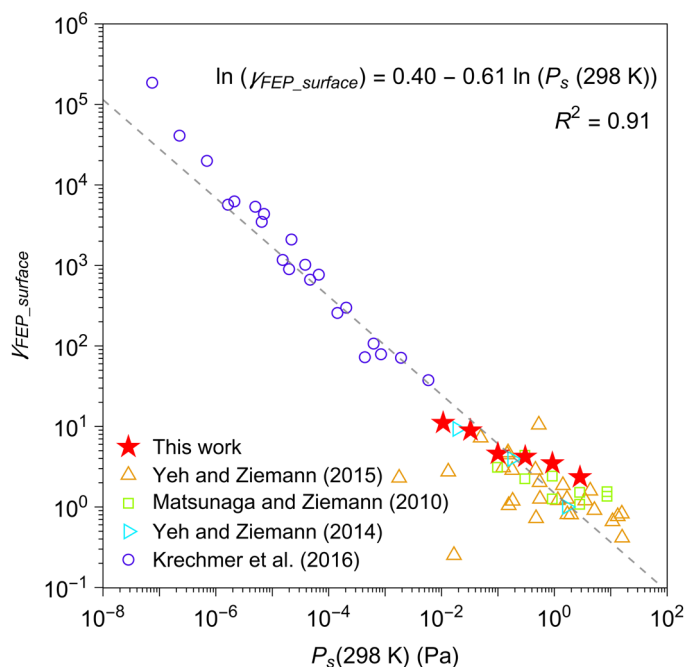
421

422 **Figure 4.** Measured values of C_{gas}/C_0 at (a) 3 hours and (b) 15 hours after injection.



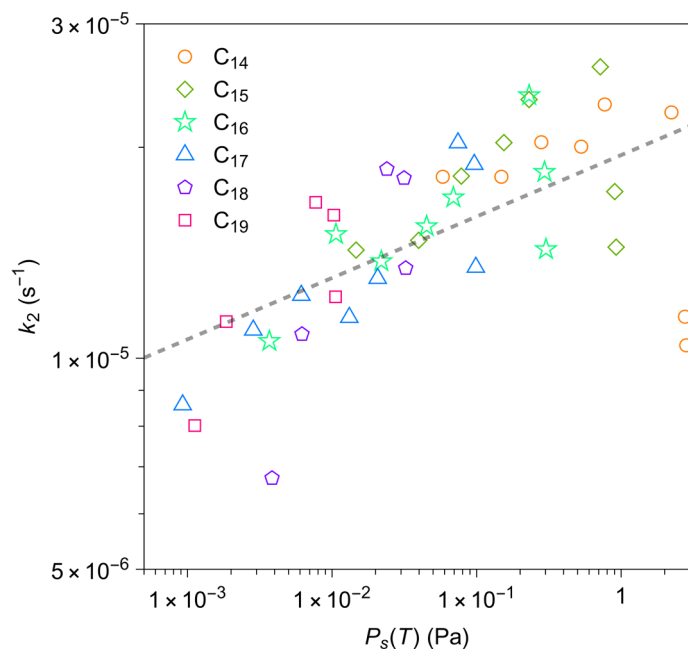
423

424 **Figure 5.** Relationships between measured ratio of concentrations in the chamber wall surface phase and in the gas phase at
 425 quasi-equilibrium and calculated values of $RT/P_s(T)$ for individual n -alkanes. Calculation methods for $C_{surface}/C_{gas}$ is
 426 detailed in the text. The values of $RT/P_s(T)$ for each n -alkane were calculated by the EVAPORATION group contribution
 427 method (Compernelle et al., 2011). The black dashed lines are linear least-squares that fit the data for each n -alkane.



428

429 **Figure 6.** Activity coefficient ($\gamma_{FEP_surface}$) of organic compounds in FEP film. The sources of data include this work and the
 430 literature (compiled by Huang et al. (2018b), including Matsunaga and Ziemann (2010), Yeh and Ziemann (2014, 2015), and
 431 Krechmer et al. (2016)). A list of chemical species that were investigated by each study is available in Table S4. Saturation
 432 vapor pressures at 298 K ($P_s(298\text{ K})$) were estimated by EVAPORATION (Compernelle et al., 2011).



433

434 **Figure 7.** Relationship between calculated first-order loss rate k_2 for each n -alkane and calculated values of saturation vapor
 435 pressure by the EVAPORATION group contribution method (Compernelle et al., 2011). The calculation method for k_2 is
 436 detailed in the text. The black dashed line is a linear least-squares fit to the data in a logarithmic scale.